Assessing white matter microstructure of the newborn with multi-shell diffusion MRI and biophysical compartment models

Article *in* NeuroImage · March 2014

DOI: 10.1016/j.neuroimage.2014.03.057 · Source: PubMed

CITATIONS
104

READS
188

8 authors, including:

Nicolas Kunz
École Polytechnique Fédérale de Lausanne
29 PUBLICATIONS **478** CITATIONS
SEE PROFILE

Hui Zhang
Shanghai University of Engineering Science
170 PUBLICATIONS **4,994** CITATIONS
SEE PROFILE

Lana Vasung
Boston Children's Hospital/Harvard Medical School, Boston, United States
61 PUBLICATIONS **1,166** CITATIONS
SEE PROFILE

Kieran O'Brien
University of Geneva
19 PUBLICATIONS **540** CITATIONS
SEE PROFILE

NeuroImage 96 (2014) 288–299

Contents lists available at ScienceDirect

NeuroImage

journal homepage: www.elsevier.com/locate/ynimg

Assessing white matter microstructure of the newborn with multi-shell diffusion MRI and biophysical compartment models

Nicolas Kunz [a,*], Hui Zhang [b], Lana Vasung [a], Kieran R. O'Brien [c], Yaniv Assaf [d,e], François Lazeyras [c], Daniel C. Alexander [b], Petra S. Hüppi [a]

[a] Division of Development and Growth, Department of Pediatrics, University of Geneva, Geneva, Switzerland
[b] Centre for Medical Image Computing and Department of Computer Science, University College London, Gower Street, London WC1E 6BT, United Kingdom
[c] Radiology-CIBM, Geneva University Hospitals, Geneva, Switzerland
[d] Department of Neurobiology, Faculty of Life Sciences, Tel Aviv University, Tel Aviv, Israel
[e] Sagol School of Neuroscience, Tel Aviv University, Tel Aviv, Israel

ARTICLE INFO

Article history:
Accepted 21 March 2014
Available online 28 March 2014

Keywords:
White matter
Microstructure
Newborn
Maturation
Myelin
Intra-neurite space
Intra-axonal space
MRI
CHARMED
NODDI
DTI
Corpus callosum
Internal capsule
Periventricular crossroads of pathways

ABSTRACT

Brain white matter connections have become a focus of major interest with important maturational processes occurring in newborns. To study the complex microstructural developmental changes in-vivo, it is imperative that non-invasive neuroimaging approaches are developed for this age-group.

Multi-b-value diffusion weighted imaging data were acquired in 13 newborns, and the biophysical compartment diffusion models CHARMED-light and NODDI, providing new microstructural parameters such as intra-neurite volume fraction (v_{in}) and neurite orientation dispersion index (ODI), were developed for newborn data. Comparative analysis was performed and twenty ROIs in the white matter were investigated. Diffusion tensor imaging and both biophysical compartment models highlighted the compact and oriented structure of the corpus-callosum with the highest FA and v_{in} values and the smallest ODI values. We could clearly differentiate, using the FA, v_{in} and ODI, the posterior and anterior internal capsule representing similar cellular structure but with different maturation (i.e. partially myelinated and absence of myelin, respectively). Late maturing regions (external capsule and periventricular crossroads of pathways) had lower v_{in} values, but displayed significant differences in ODI. The compartmented models CHARMED-light and NODDI bring new indices corroborating the cellular architectures, with the lowest v_{in}, reflecting the late maturation of areas with thin non-myelinated fibers, and with highest ODI indicating the presence of fiber crossings and fanning.

The application of biophysical compartment diffusion models adds new insights to the brain white matter development in vivo.

Introduction

While the majority of the brain cellular components are established prior to birth, postnatal development is marked by their maturation and reorganization (Kostović et al., 2014). Differentiation of neuronal types, dendritic arborization, axonal ingrowth, outgrowth and retraction, synaptogenesis and myelination are the most pronounced processes spanning from the late prenatal period to the first three years of life and beyond (Brody et al., 1987; Judaš, 2011; Kang et al., 2011; Miller et al., 2012; Penny, 2012; Yakovlev and Lecours, 1967). Development and establishment of axonal pathways, pre-myelination and final myelination of fiber bundles, are one of the most intriguing research fields in human neurobiology. Establishment of axonal pathways, usually encompassing overproduction and retraction, is hierarchically organized and spans from early fetal to early postnatal period (Kostovic and Jovanov-Milosevic, 2006; Vasung et al., 2010). It is followed by axonal myelination that starts in central regions and progresses towards the poles (Brody et al., 1987; Flechsig Of Leipsic, 1901; Judaš et al., 2011; Miller et al., 2012; Yakovlev and Lecours, 1967), beginning in the last trimester of pregnancy but continuing until early adolescence (Paus et al., 2001; Yakovlev and Lecours, 1967). Modification of these early establishments of brain microstructural networks has been linked to many neurodevelopmental and neuropsychiatric disorders both in childhood and adulthood (Bullmore and Sporns, 2009). To study the duration, complexity, and species-specific features of brain microstructural development processes properly, it is imperative that noninvasive methodological approaches within the field of neuroimaging are developed for these specific time periods.

Diffusion magnetic resonance imaging (dMRI) has demonstrated its unique ability to non-invasively investigate cellular architecture of the

* Corresponding author at: Centre d'Imagerie BioMedicale (CIBM-AIT), Ecole Polytechnique Fédérale de Lausanne (EPFL), Station 6, CH-1015 Lausanne, Switzerland.
E-mail address: nicolas.kunz@epfl.ch (N. Kunz).

http://dx.doi.org/10.1016/j.neuroimage.2014.03.057

developing human brain. dMRI is considered today as a safe and suitable technique for studying the human fetal and neonatal brain (Hüppi and Dubois, 2006). Diffusion tensor imaging (DTI) parameters have been shown to depict the early organization of white matter fiber bundles (Baratti et al., 1999; Huang et al., 2012; Hüppi et al., 1998; Neil et al., 1998), to follow brain maturation (Forbes et al., 2002; Gilmore et al., 2007; Provenzale et al., 2010) and to be of great utility in probing brain injury (Hüppi et al., 2001; Inder et al., 1999; Vasung et al., 2013). Despite the valuable information that DTI provides about the general organization and maturation of fiber bundles, the interpretation of the changes on a cellular scale remains very challenging (Pierpaoli et al., 1996). For example, it remains impossible with DTI to differentiate myelination from compaction or an increase in number of fibers, which all would result in an increase of FA (Beaulieu, 2009).

Recent advances in dMRI present new opportunities to examine brain development. Using biophysical models of brain tissues it is possible to relate diffusion-weighted signals directly to the underlying cellular microstructure (Alexander et al., 2010; Assaf and Basser, 2005; Barazany et al., 2009; Behrens et al., 2003; Stanisz et al., 1997; Zhang et al., 2011, 2012). Of particular interest are two techniques, CHARMED and NODDI, which are suitable for implementation in routine clinical protocol.

They utilize, within the DW signal, diverse representations of brain cellular compartments based on the local diffusion process, such as restriction, hindrance or free diffusion. Stanisz et al. (1997) divided the diffusion signal into three compartments representing different central nervous system cell types. They proposed a sphere for the glial cells and ellipsoids for the axons with water exchanging between the intra- and extra-axonal compartments. Following this work, several models, focusing on a better representation of the axonal space, have been published: (i) Axon modeling by parallel sticks (Behrens et al., 2003); (ii) composite hindered and restricted model of diffusion (CHARMED), which represents the intra-axonal space by parallel cylinders with radii following a gamma distribution (Assaf and Basser, 2005); and (iii) other models that go further by fitting the axonal diameter distribution (Barazany et al., 2009) or using a single index of the diameter distribution in the ActiveAx technique (Alexander et al., 2010; Zhang et al., 2011). All these models are potentially more sensitive to cellular microstructure and able to extract parameters of the cellular geometry, axonal density and axonal diameter. However, their wide adoption is limited by demanding hardware requirements, such as high maximum gradient strength (>60 mT/m), and/or long acquisition time (Alexander et al., 2010; Dyrby et al., 2013).

To overcome this problem of implementation on clinical systems, Zhang et al. (2012) recently proposed a new compartment model called neurite orientation dispersion and density imaging (NODDI) that extends the study of brain tissue microstructure from white matter to gray matter (GM) in the adult brain. The NODDI model introduces an orientation dispersion index (ODI) to model the dispersion/fanning of the axonal fibers or dendrites. As a result, the NODDI model can additionally be used to investigate the dendritic packing and arborization as done for example in GM (Jespersen et al., 2012; Winston et al., 2014). The extension of the biophysical diffusion model to less coherent cellular structure such as found in GM supports the application to the immature newborn brain. Furthermore, it has been demonstrated in the adult brain, that intra-neurite volume fraction (ν_{in}) and ODI were able to disentangle the microstructural effects underlying FA with an acquisition time comparable to conventional DTI.

The new cellular microstructural parameters derived from CHARMED and NODDI models, such as ν_{in} and ODI, have the potential to provide new markers to study the complex process of human brain development. However, to the best of our knowledge, these techniques have yet to be applied to the immature brain. The present study aims to establish the feasibility and utility of these two techniques in neonatal imaging. Our specific objectives were to: 1. Demonstrate the feasibility of multi-b-value shell DWI acquisition and the application of biophysical compartment diffusion model in human newborns. 2. Establish the most suitable model for a neonatal study. 3. Establish normative parameter values of biophysical compartment models in newborns at term. 4. Compare fiber bundles with different stage of maturation and to corroborate findings to current knowledge from previous histology studies (Brody et al., 1987; Judaš, 2011; Miller et al., 2012; Yakovlev and Lecours, 1967). In order to establish the most suitable model for neonatal study, two biophysical compartment models, with different levels of complexity, were compared to each other and to conventional DTI: 1. a white matter model, "CHARMED-light", estimating the intra-axonal fraction, which is based on CHARMED (Assaf and Basser, 2005) but adopts various simplifications that are used in the NODDI model; and 2. a whole brain model, NODDI (Zhang et al., 2012), estimating the intra-neurite volume fraction, the intra-voxel axonal orientation dispersion, and signal fraction from free water. A preliminary version of this work was reported in Kunz et al. (2013).

Materials and methods

Subjects

Thirteen newborns (gestational age at birth: 30 to 40 weeks) were scanned at term (40th week of gestation). All the infants were scanned in natural sleep without sedation. Heart rate and blood saturation were monitored transcutaneously in the MR scanner. The newborns were tightly wrapped and positioned in a vacfix pillow. Special ear muffs were used to protect them from scanner acoustic noise. This study was performed in agreement with the local ethical committee and parents gave their written informed consent.

MR acquisition

All imaging was conducted on a Magnetom 3T TimTrio Siemens system (Erlangen, Germany) using a 32-channel head coil. First, high-resolution T_2 weighted anatomical images were acquired in order to identify the main brain structures to position the slices of the DW images. T_2-weighted images were acquired using a turbo spin-echo (TE/TR = 150/4600 ms, acquisition time = 5 min 30 sec) with an in-plane resolution of 0.8×0.8 mm^2 and a slice thickness of 1.2 mm.

A multi-b-value shell DWI protocol was acquired using a single shot echo-planar sequence, with the twice refocused spin-echo and diffusion encoding scheme to minimize eddy-current induced distortions (Reese et al., 2003). The acquisition parameters were: TE/TR = 93/3500 ms, acquisition matrix 80×80, resolution of $2 \times 2 \times 2$ mm^3, with 22 slices centered on the corpus callosum (CC). A total of 66 DWI were acquired, three of them were b_0 reference images. The remaining 63 were separated in 5 shells with the following distribution (# of directions/b-value in s/mm^2): 6/50; 9/250; 12/700; 16/1400; and 20/2500. All 63 directions were non-collinear and were uniformly distributed in each shell (Assaf and Basser, 2005). The acquisition time was 4 min.

Data preprocessing

Prior to reconstruction, slices corrupted by motion were excluded from the analysis with an in-house automated procedure based on signal intensity drop. Exclusion was verified with visual inspections for false positive and negative. On average 2.5% of the total number of slices were discarded per subject. A diagrammatic representation of the full data-processing pipeline is presented in Fig. 1.

DTI

Diffusion tensor (DT) was reconstructed for each subject with Camino (Cook et al., 2006) using a linear regression to the logarithm of the measurement algorithm (Basser et al., 1994). To mimic conventional DTI, performed usually with a single b-value of 1000 s/mm^2,

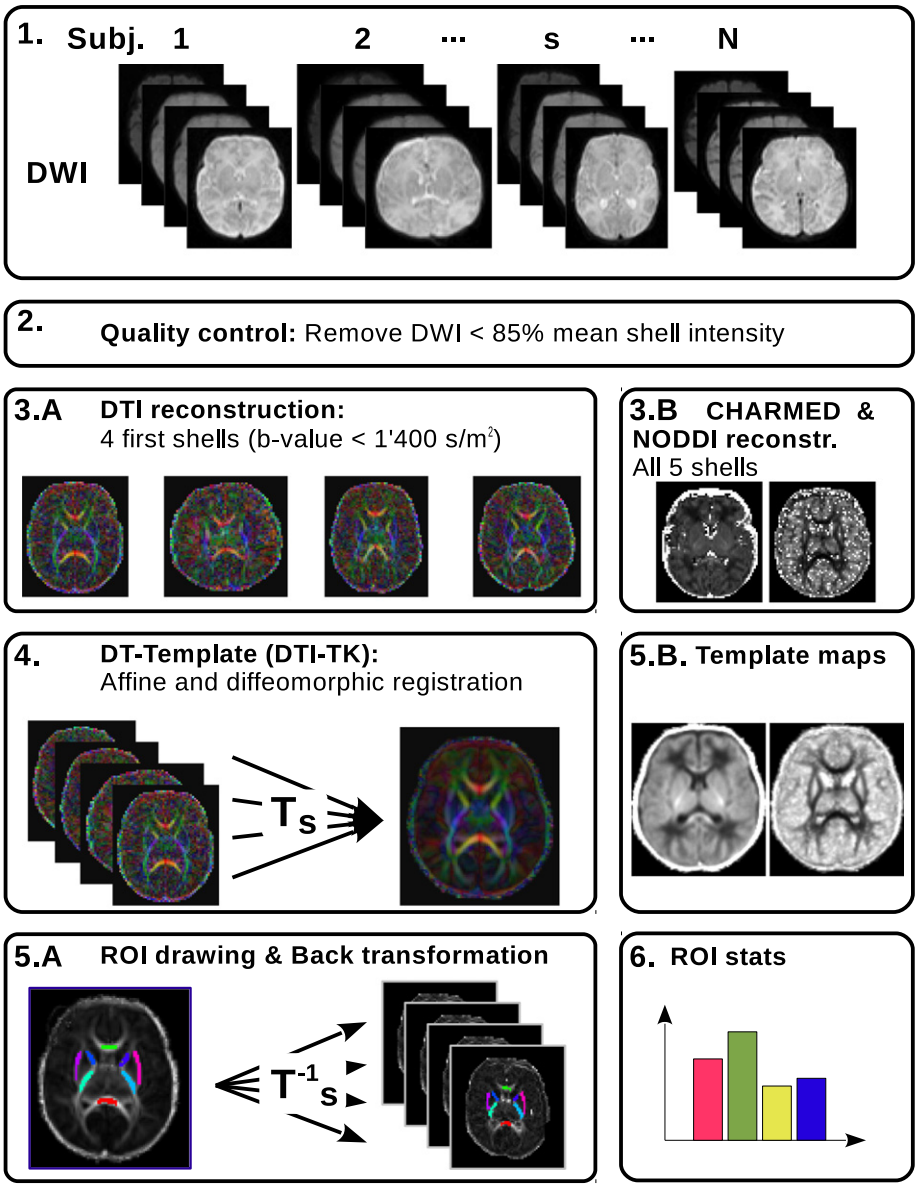

Fig. 1. Data processing diagram. 1. After acquisition DWI are sent to 2. a quality control routine. 3. A Diffusion tensor is reconstructed and used to 4. generate a study-specific DT-template. 5. ROIs are drawn manually on the template and then back transformed to the subject space to then 6. performed statistics. 3.B In parallel, the same data-sets are used to reconstruct CHARMED and NODDI. 5. B Transformation estimated in 4. can be used to create subject average model derived parameter scalar maps.

only the first four shells were used limiting the maximum b-value to 1400 s/mm^2 and the number of diffusion directions to 43. The usual DT metrics were calculated; the fractional anisotropy (FA), the mean diffusivity (MD) given by the mean value of the three eigenvalues, the axial diffusivity (AD) equal to the highest eigenvalue and the radial diffusivity (RD) equal to the mean of the second and third eigenvalue.

CHARMED-light

The CHARMED-light model is a simplified version of the CHARMED model proposed by Assaf and Basser (2005). It is composed of three compartments: restricted, hindered and isotropic compartments. The restricted compartment, which represents the intra-axonal space (v_{ia}), is modeled as sticks. The sticks capture the highly restricted diffusion perpendicular to the axons with a perpendicular diffusivity equal to 0 and free diffusion along the neurite with a longitudinal diffusivity equal to 2×10^{-3} mm^2/s.

The hindered compartment, which represents the extra-axonal space (ea), is modeled as a cylindrically symmetric tensor. The principal diffusion direction of the tensor is aligned with the intra-axonal compartment and with an equal longitudinal diffusivity of 2×10^{-3} mm^2/s. The radial diffusivity was estimated using the tortuosity model where RDea $= (1 - v_{ia})$Dea (Szafer et al., 1995), as adopted in the NODDI model (Zhang et al., 2012). Finally, the diffusivity of the isotropic compartment was fixed to the one of free water 3×10^{-3} mm^2/s to model the CSF while the volume fraction was defined as v_{iso}. The DW signal was thus modeled using the following equation:

$$S/S_0 = (1-v_{iso}) \cdot (v_{ia} \cdot S_{ia} + (1-v_{ia}) \cdot S_{ea}) + v_{iso} \cdot S_{iso}. \quad (1)$$

The model for the signal thus has three components: the intra-axonal signal (S_{ia}), the extra-axonal signal (S_{ea}) and the isotropic signal (S_{iso}). The extra-axonal volume fraction (v_{ea}) by definition is equal to $(1-v_{ia})$. A total of 4 parameters were estimated, with v_{ia}, v_{iso} and two angles defining the fiber orientation.

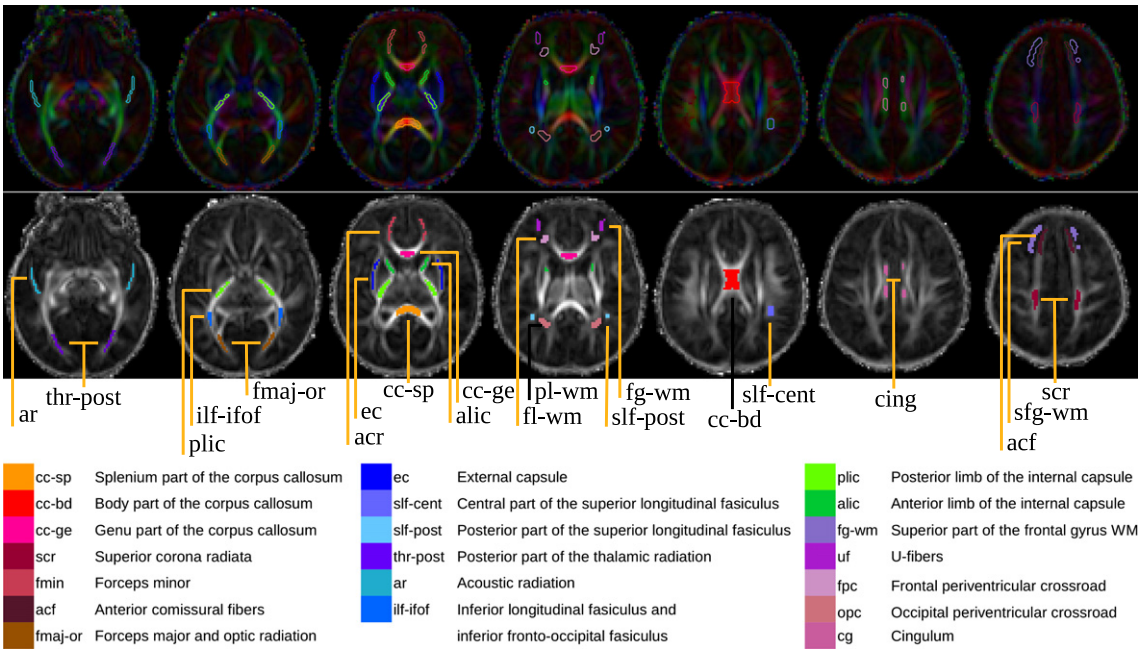

Fig. 2. Mean RGB and FA maps of the study-specific DT template over the 13 subjects with the 20 white matter ROIs overlaid (top and bottom row respectively).

NODDI

The NODDI model provides a unified model for gray and white matter microstructure. It uses the same compartmentalization as the CHARMED-light model, i.e. restricted, hindered and isotropic, but adopts the Watson distribution to model the orientation distribution of the sticks (Zhang et al., 2012). The Watson distribution enables the modeling of highly coherent white matter tracts, as CHARMED, as well as highly dispersed structures such as dendritic aborization in GM. Therefore in contrast to CHARMED, the restricted compartment represents both the axons and dendrites and is described through intra-neurite volume fraction (v_{in}). The dispersion of the sticks is summarized by the scalar-valued orientation dispersion index (ODI), which brings the total number of parameters estimated in this model to five.[1]

$$S/S_0 = (1-v_{iso}) \cdot (v_{in} \cdot S_{in} + (1-v_{in}) \cdot S_{en}) + v_{iso} \cdot S_{iso} \quad (2)$$

The model for the signal thus has three components: the intra-neurite signal (S_{in}), the extra-neurite signal (S_{en}) and the isotropic signal (S_{iso}). The extra-neurite volume fraction (v_{en}) by definition is equal to ($1 - v_{in}$). A total of 5 parameters were estimated, with v_{in}, v_{iso}, ODI and two angles defining the fiber orientation.

Both CHARMED-light and NODDI models were fitted using the NODDI toolbox.[1]

Model comparison and correlation

The fitting quality of the different models was estimated voxelwise using the Bayesian information criterion (BIC) over all the 66 directions for all three-reconstruction models, to account for the differences of complexity of the tested models (Penny, 2012). BIC model scores were ranked voxelwise and the average model goodness-of-fit ranking over the different ROIs was computed (BICrk), showing the fraction of pixels in each region in which the BIC ranks the model (1st/2nd/3rd).

Inter-model parameter correlations were estimated using a Spearman's rank correlation coefficient.

[1] NODDI Matlab toolbox, http://www.nitrc.org/projects/noddi_toolbox/

Normative parameter maps of CHARMED and NODDI

The diffusion tensor (DT) was spatially normalized to the study-specific DT template using DTI-TK (Zhang et al., 2006). The regions of interest (ROI) were drawn on the DT study-specific template and were then transformed back to the subject space in order to compute ROI-averaged estimates of DTI, CHARMED and NODDI maps. Twenty different white matter regions were identified on the DT-template (Fig. 2).

Markers of newborn white matter maturation

Region specific differences were tested pair-wise using a non-parametric Mann–Whitney test and Bonferroni correction was applied to take into account the multitude of statistical testing involving multiple ROIs and multiple parameters of each model. Based on a significance threshold of 0.05 and after correction for multiple comparison, the significance thresholds for p-value are equal to $0.05 / (20 \cdot \cdot) = 0.0006$ for DTI and NODDI and $0.05 / (20 \cdot \cdot) = 0.0008$ for CHARMED-light.

Results

The optimized multi-b-value shell protocol was successfully implemented on a 3T clinical system and the optimized maximal b-value of 2500 s/mm^2 resulted in an acceptable TE of 93 ms, ensuring a good SNR of 20 ± 2 over the 13 subjects in the b_0 images. All datasets were successfully reconstructed with the three models (DT, CHARMED-light and NODDI) and show comparable fitting quality (Fig. 3 and Table 1). On average, only 2.5% of the slices per subject were discarded during the quality control routine based on significant signal loss due to motion artifact.

Model comparison and correlation

After ranking the BIC score on a pixel-based, NODDI clearly distinguishes itself in all ROIs; the differentiation between CHARMED-light and DTI is less clear (Table 1, BICrk).

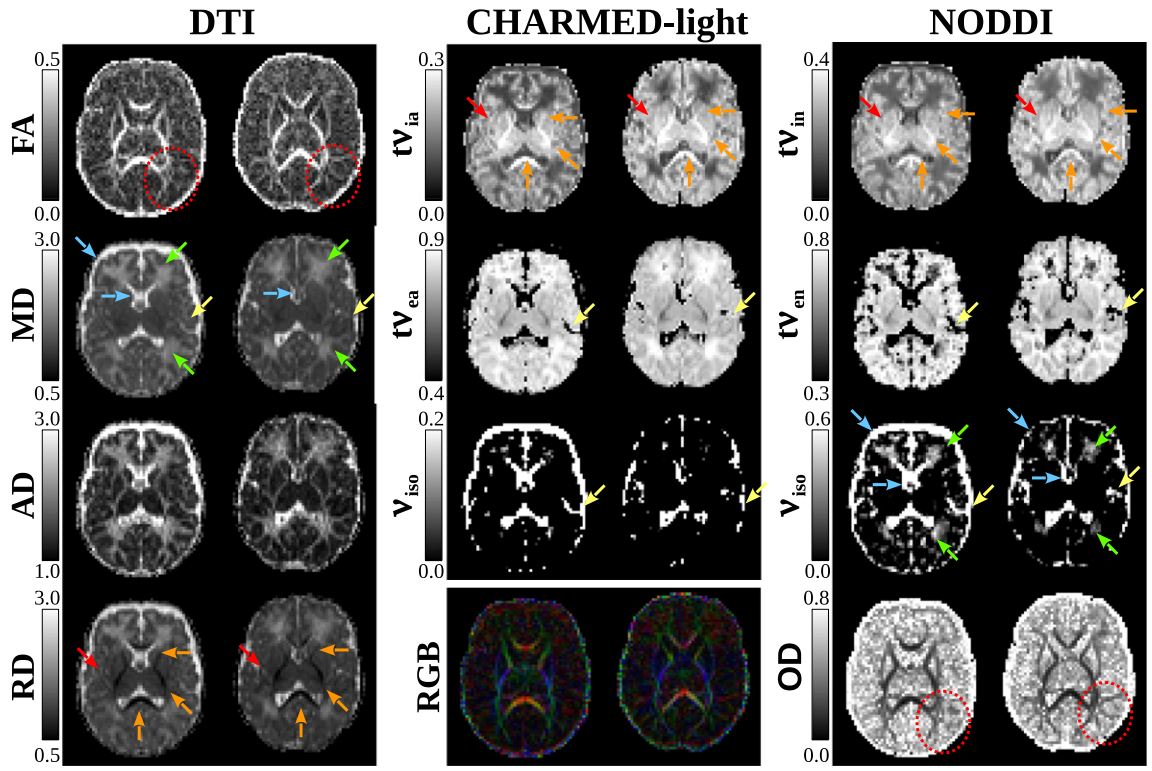

Fig. 3. Scalar maps from two typical subjects for the three reconstruction model DT, CHARMED-light and NODDI (form left to right). The intra-and extra-axonal/neurite volume fraction maps ($tv_{ia/n}$ and $tv_{ea/n}$) were weighted by the isotropic volume fraction ($1 - v_{iso}$) for a better rendering. Orange arrows: corpus callosum and internal capsule; ref arrows: external capsule; blue arrows: CSF and ventricles; yellow arrow: Sylvian fissure; green arrows: periventricular crossroads of pathways; red dotted circle: cortical projection.

As expected from their analogous conception, CHARMED-light v_{ia} values were consistent with NODDI v_{in} (Fig. 4). However, by not modeling the effect of fiber dispersion, CHARMED-light underestimates v_{ia} compared to NODDI.

Consistent with the findings in the adult brain, fractional anisotropy measured from DTI shows the strongest correlation with the orientation dispersion index of NODDI (Fig. 4). In contrast, FA values show weaker correlation to CHARMED-light v_{ia} and even lower values in correlation to NODDI v_{in} (Fig. 4). The v_{ia} and v_{in} show the strongest correlation to the DTI RD (Fig. 4). No correlation was found between the DTI axial diffusivity and compartment model derived parameters (data not shown).

Normative scalar parameter template maps and values

Subject's DT images were all registered together into a study-specific template using DTI-TK (Zhang et al., 2006). The resulting DT template was of excellent quality and all main fiber tracts of the human newborn were clearly identifiable (Figs. 3 & 5). The template was reconstructed with an isotropic resolution of 1.3 mm^3 allowing the accurate delineation of 20 WM ROIs (Fig. 2). The same estimated spatial transformations from subject's space to study-specific DT template space were used to generate the scalar template maps of the biophysical compartment models CHARMED-light and NODDI. The resulting scalar template maps were of good quality and resulted in high resolution maps of the newborn brain white matter cellular micro-structures (Fig. 5).

The intra-axonal/neurite volume fraction maps calculated from CHARMED-light and NODDI showed very similar pattern. They were overall consistent to the known newborn brain anatomy: the highest values occurred in the main white matter tracts of the newborn (i.e. cc and plic, orange arrows in Figs. 3 & 5) and in general higher values were found in the white matter tracts than in the gray matter. A few regions break that rule, the external capsule (ec, red arrow, Figs. 3 & 5) and the frontal and occipital periventricular crossroads of pathways (fcp and ocp, green arrows Figs. 3 & 5) show lower $v_{ia/n}$ values than GM. In the DT maps, the same regions (ec, fcp and ocp) were also highlighted in the diffusivity maps with high AD and RD values, which is consistent with a large extra-neurite space or in other words a small intra-neurite space.

The isotropic volume fraction maps of both CHARMED-light and NODDI allow a clear delineation of the CSF-filled space such as the ventricles (blue arrows, Figs. 3 & 5). CSF contamination was also seen in the superior portion of the Sylvian fissure (yellow arrows, Figs. 3 & 5). NODDI v_{iso} maps show also some significant contribution in the periventricular areas (fcp and ocp, green arrows Figs. 3 & 5).

In the ODI maps from NODDI, the main newborn white matter tracts are revealed as regions with very low dispersion. The white matter tracts are highlighted by ODI and FA in a similar way, but with an inverted contrast (red dashed ellipse, Figs. 3 & 5).

Markers of newborn white matter maturation

The statistically-significant regional differences of selected parameters are shown in Fig. 6 and the mean ROIs values of all the derived parameters are summarized in Table 1.

White matter regions containing projectional and callosal fibers

Early maturing fiber bundles were clearly highlighted in the intra-axonal/neurite volume fraction of CHARMED-light and NODDI template scalar maps (Fig. 5). Indeed, the central callosal fibers (splenium, genu and body part of the corpus callosum, cc-sp, -ge and -bd, respectively) and regions containing majority of the projection fibers (within posterior and anterior limb of the internal capsule, plic and alic respectively) show the highest $v_{ia/n}$ values compared to almost all other areas (exceptions: CHARMED-light — alic vs. ec and ilf-ifof; NODDI — alic vs. ec and thr-post). FA, ODI and $v_{ia/n}$ of CHARMED-light and NODDI all distinguish

Table 1
Mean model derived parameter values over the 13 subjects in the 20 WM ROIs for the 3 investigated reconstruction methods (DTI, CHARMED-light and NODDI).

	DTI					CHARMED			NODDI			
	FA	MD	AD	RD	BICrk	v_{ia}	v_{iso}	BICrk	v_{in}	v_{iso}	ODI	BICrk
cc-sp	0.61 ± 0.03	1.28 ± 0.06	2.30 ± 0.06	0.77 ± 0.07	9/45/45	0.33 ± 0.02	0.09 ± 0.04	0/45/55	0.45 ± 0.03	0.17 ± 0.04	0.13 ± 0.02	91/9/0
cc-bd	0.46 ± 0.05	1.37 ± 0.12	2.11 ± 0.12	1.00 ± 0.14	0/28/72	0.29 ± 0.03	0.14 ± 0.08	0/72/28	0.45 ± 0.06	0.26 ± 0.11	0.20 ± 0.04	100/0/0
cc-ge	0.54 ± 0.05	1.35 ± 0.07	2.25 ± 0.09	0.89 ± 0.09	5/44/51	0.27 ± 0.03	0.07 ± 0.03	0/51/49	0.38 ± 0.03	0.18 ± 0.05	0.15 ± 0.02	95/5/0
scr	0.28 ± 0.05	1.34 ± 0.13	1.73 ± 0.09	1.15 ± 0.16	0/100/0	0.18 ± 0.04	0.00 ± 0.01	0/0/100	0.23 ± 0.03	0.02 ± 0.06	0.31 ± 0.06	100/0/0
fmin	0.20 ± 0.03	1.62 ± 0.12	1.95 + 0.11	1.45 ± 0.13	0/24/76	0.12 + 0.02	0.01 ± 0.02	0/76/24	0.20 ± 0.02	0.13 + 0.10	0.44 ± 0.09	100/0/0
acf	0.19 ± 0.03	1.45 ± 0.16	1.71 ± 0.16	1.33 ± 0.16	0/61/39	0.15 ± 0.03	0.01 ± 0.02	0/39/61	0.22 ± 0.02	0.08 ± 0.09	0.49 ± 0.06	100/0/0
fmaj-or	0.32 ± 0.03	1.37 ± 0.09	1.86 ± 0.08	1.13 ± 0.10	0/83/17	0.18 ± 0.03	0.00 ± 0.00	0/17/83	0.23 ± 0.03	0.02 ± 0.02	0.26 ± 0.03	100/0/0
plic	0.50 ± 0.02	1.03 ± 0.04	1.68 ± 0.05	0.71 ± 0.04	3/97/0	0.33 + 0.02	0.00 ± 0.00	0/0/100	0.39 ± 0.03	0.01 ± 0.01	0.17 ± 0.01	97/3/0
alic	0.37 ± 0.04	1.17 ± 0.05	1.68 ± 0.06	0.91 ± 0.06	0/100/0	0.25 ± 0.02	0.00 ± 0.00	0/0/100	0.30 ± 0.03	0.01 ± 0.01	0.22 ± 0.02	100/0/0
ilf-ifof	0.39 ± 0.04	1.34 ± 0.10	1.96 ± 0.08	1.03 ± 0.11	0/75/25	0.20 ± 0.03	0.01 ± 0.02	0/25/75	0.26 ± 0.04	0.05 ± 0.05	0.20 ± 0.02	100/0/0
ec	0.28 ± 0.03	1.23 ± 0.07	1.58 ± 0.06	1.05 ± 0.08	14/86/0	0.21 ± 0.02	0.00 ± 0.00	0/0/100	0.27 ± 0.03	0.00 ± 0.00	0.32 ± 0.02	86/14/0
slf-cent	0.27 ± 0.04	1.36 ± 0.10	1.70 ± 0.08	1.19 ± 0.12	0/96/4	0.17 ± 0.03	0.00 ± 0.00	0/4/96	0.23 ± 0.03	0.03 ± 0.04	0.33 ± 0.06	100/0/0
slf-post	0.22 ± 0.03	1.51 ± 0.10	1.83 ± 0.12	1.35 ± 0.10	0/67/33	0.13 ± 0.03	0.00 ± 0.00	0/33/67	0.19 ± 0.02	0.07 ± 0.05	0.38 ± 0.05	100/0/0
thr-post	0.27 ± 0.04	1.46 ± 0.18	1.86 ± 0.20	1.26 ± 0.18	0/87/13	0.19 ± 0.05	0.06 ± 0.08	0/13/87	0.29 ± 0.08	0.15 ± 0.14	0.34 ± 0.06	100/0/0
ar	0.21 ± 0.01	1.37 ± 0.10	1.65 ± 0.11	1.23 ± 0.10	0/84/16	0.16 ± 0.03	0.00 ± 0.00	0/16/84	0.23 ± 0.03	0.04 ± 0.04	0.40 ± 0.03	100/0/0
fg-wm	0.14 ± 0.01	1.27 ± 0.06	1.45 ± 0.07	1.18 ± 0.06	0/88/12	0.18 ± 0.02	0.00 ± 0.01	0/12/88	0.26 ± 0.02	0.04 ± 0.04	0.57 ± 0.03	100/0/0
uf	0.15 ± 0.02	1.34 ± 0.07	1.55 ± 0.08	1.24 ± 0.07	12/74/15	0.17 ± 0.02	0.00 ± 0.01	0/15/85	0.24 ± 0.03	0.04 ± 0.03	0.54 ± 0.05	88/12/0
fpc	0.13 ± 0.01	1.80 ± 0.10	2.04 ± 0.11	1.69 ± 0.10	0/0/100	0.09 ± 0.01	0.05 ± 0.06	0/100/0	0.22 ± 0.04	0.31 ± 0.13	0.62 ± 0.06	100/0/0
opc	0.17 ± 0.03	1.75 ± 0.13	2.05 ± 0.11	1.59 ± 0.14	0/0/100	0.10 ± 0.01	0.05 ± 0.06	0/100/0	0.21 ± 0.04	0.27 ± 0.15	0.48 ± 0.09	100/0/0
eg	0.32 ± 0.04	1.36 ± 0.07	1.85 ± 0.07	1.12 ± 0.09	0/81/19	0.18 ± 0.02	0.00 ± 0.00	0/19/81	0.23 ± 0.02	0.02 ± 0.02	0.27 ± 0.02	100/0/0

Diffusivity values are given in 10^{-3} mm^2/s. Errors represent the standard deviation across the subjects. Model fitting quality ranking is given by BICrk.

the anterior limb of the posterior limb of the internal capsule, with higher $\nu_{ia/n}$ and FA values and lower RD and ODI for the plic.

FA and ODI show significant differences between cc-sp and cc-bd/-ge, while CHARMED-light and NODDI $\nu_{ia/n}$ show higher value in the cc-sp compared to the cc-ge values. However, no distinction was made between the cc-ge and cc-bd using any of the parameters, except RD showing higher diffusivity in the cc-bd.

Periventricular crossroads of pathways and white matter regions containing cortico-cortical associational fibers

Regions containing long association fibers (inferior longitudinal and fronto-occipital fasciculus cingulum and U-fibers; ilf-ifof, cg and uf) and also the external capsule (ec) have very close $\nu_{ia/n}$ values derived from CHARMED-light and NODDI model. Despite that they show a large spread in FA and ODI values. FA shows the highest values in ilf-ifof (containing long cortico-cortical associational fibers) followed by ec and forceps minor (fmin) afterwards (containing associational and projectional fibers) and inversely for ODI values. The $\nu_{ia/n}$ and FA showed the lowest value range in regions containing mostly the short associational U-fibers and periventricular crossroads of pathways while ODI showed the highest values for these regions. In periventricular crossroad areas differences were found between CHARMED-light and NODDI (Fig. 6). Furthermore CHARMED-light ν_{ia} made a distinction between fpc and opc. ODI showed statistically significant differences when comparing regions containing short and regions containing long associational fibers, with ilf-ifof having a low dispersion index while superior part of the frontal gyrus (fg-wm) having the highest dispersion index.

Discussion

This work demonstrates the feasibility of using multiple b-value shell dMRI with the multi-compartment diffusion models, CHARMED-light and NODDI, in non-sedated human newborns. dMRI was acquired with a maximal b-value of 2500 s/m^2, short acquisition time (4 min) and appropriate handling of the newborns. Conventional DTI reconstructions, performed on the same data-sets, were in good agreement with literature (Bashat et al., 2007; Dubois et al., 2006; Hüppi et al., 1998; Partridge et al., 2004) and were used to generate a high resolution and a study-specific DT template (Wang et al., 2011). Twenty ROIs, placed in the white matter, were investigated. All three methods highlighted the compact and oriented structure of the corpus-callosum with the highest FA and $\nu_{ia/n}$ values and the smallest ODI values. We could clearly differentiate, using the FA, $\nu_{ia/n}$ and ODI, the posterior and anterior internal capsule representing similar cellular structure but with different stage of maturation (i.e. partially myelinated and absence of myelin, respectively). Thus we were able to depict the spatio-temporal differences of the maturation of the white matter during the neonatal period.

Model comparison and correlation

The good agreement between CHARMED-light and NODDI derived parameters with the newborn cellular architecture known from histology (Brody et al., 1987; Yakovlev and Lecours, 1967) demonstrates the reliability of the application of compartmented models in the human newborn. This result is further supported by the similar contrast found between CHARMED-light and NODDI $\nu_{ia/n}$ maps (Fig. 3) demonstrating the good consistency between both models. Moreover, based on the BIC model selection, the NODDI model describes most accurately the diffusion mechanisms in white matter with one fitting parameter less than DTI. It also demonstrates the importance of the integration of the additional ODI parameters. Indeed, whereas the intra-axonal/neurite volume fractions estimated from CHARMED-light and NODDI were very similar for several ROIs (e.g. ec, ilf-ifof and fmin, Fig. 5), ODI was

Fig. 4. Inter-model metric comparisons. Scatter plot of the different derived model parameters of the 20 ROIs over the 13 subjects. Colors represent the different ROIs, see Fig. 2 for details. Rho corresponds to the correlation estimated with a Pearson test.

able to differentiate the same regions and shows the biggest number of regional differences proving the importance of modeling fiber dispersion to obtain high sensitivity to cellular microstructure. Similarly, as already confirmed in adults (Zhang et al., 2012), by modeling the intra-voxel fiber dispersion it avoids the under estimation of the intra-axonal volume fraction of the CHARMED-light model (Fig. 5) as illustrated in the fpc and opc regions (Fig. 6).

The model derived parameter correlation provides some new insights on the underlying contribution of the fractional anisotropy. In agreement with the findings in the adult brain (Zhang et al., 2012), the FA can be disentangled into two independent contributions: i) the neurite density (ν_{in}) with a weak positive correlation; and ii), the axonal orientation dispersion (ODI) with a strong negative correlation (Fig. 5). The intra-axonal/neurite volume fraction shows stronger correlation to the radial diffusivity, which was also reported with a more complex model that estimates the axon diameters (Alexander et al., 2010).

Markers of newborn white matter maturation

One of the principal aims of our study was to identify new biomarkers of white matter maturation in the developing human brain using new approaches in diffusion magnetic resonance imaging. Several previous studies were able to assess the maturation of the white matter (Bashat et al., 2007; Dubois et al., 2006; Hüppi et al., 1998; Partridge et al., 2004) but only by assessing the FA and ADC values of dMRI. With the new approach proposed here we were able to depict the components of the white matter microstructure (intra- and extra-neurite compartments) and their geometrical organizations (dispersion level) that contribute to the FA changes of the white matter during the neonatal period. One of the hallmarks of postnatal white matter maturation is retraction and myelination of the axonal pathways. Retraction and reorganization of prenatally established axonal pathways (LaMantia and Rakic, 1990) are one of the main factors contributing to the changes in geometrical organization of the axons.

Myelination of axonal pathways, on the other hand, is a long lasting process (Miller et al., 2012). It starts in central regions and continues outward to the poles, with posterior sites preceding the fronto-temporal (Brody et al., 1987; Yakovlev and Lecours, 1967). As a result, only the posterior limb of internal capsule is partially myelinated at term while association fibers (e.g. ilf-fifo and fg-min) and periventricular areas (fpc and opc) mature postnatally (Brody et al., 1987; Judaš et al., 2011; Kostović et al., 2014; Miller et al., 2012; Yakovlev and Lecours, 1967).

Compared to the anterior limb of the internal capsule, all three methods used in this study identified the myelinated fibers of the plic that had significantly higher FA and $\nu_{ia/n}$ compared to the alic (composed out of the projectional cortico-basal ganglia and thalamocortical

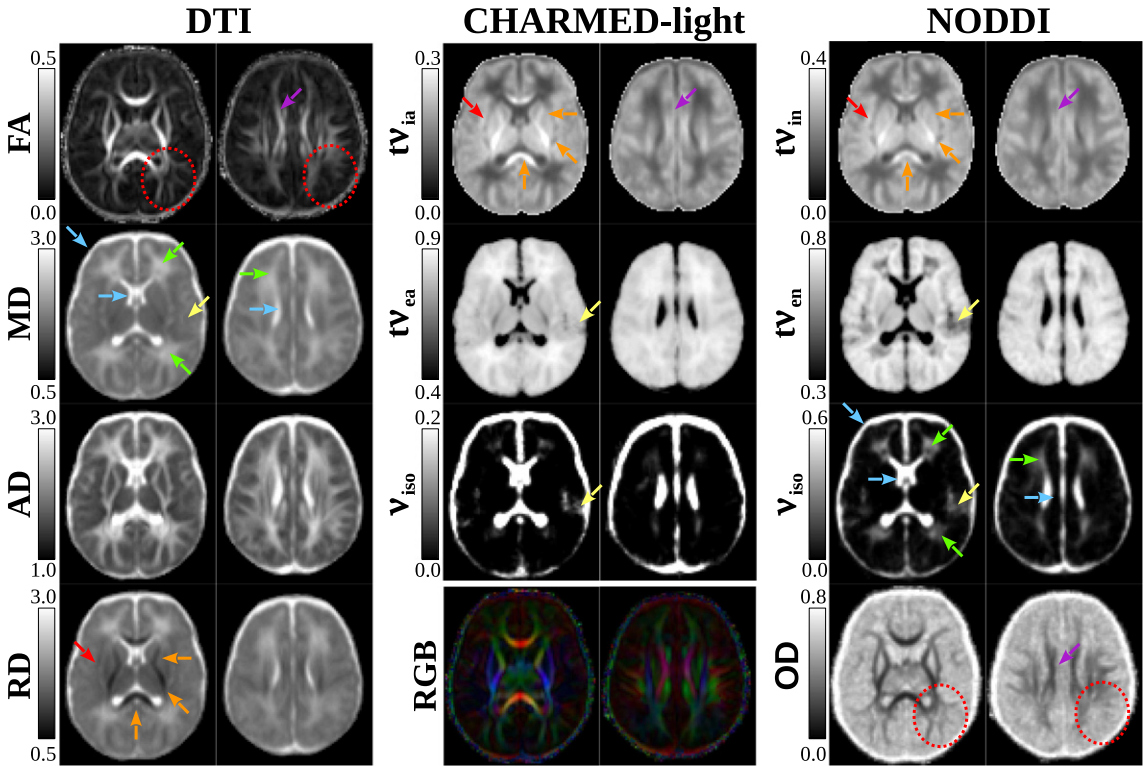

Fig. 5. Study-specific template scalar maps for the three reconstruction models DT, CHARMED-light and NODDI (form left to right). The intra-and extra-axonal/neurite volume fraction maps ($t\nu_{ia/n}$ and $t\nu_{ea/n}$) were weighted by the isotropic volume fraction ($1-\nu_{iso}$) for a better rendering. Orange arrows: corpus callosum and internal capsule; ref arrows: external capsule; blue arrows: CSF and ventricles; yellow arrow: Sylvian fissure; green arrows: periventricular crossroads of pathways; red dotted circle: cortical projection.

fibers of the frontal lobe). Our results suggest that plic (composed out of the earliest maturing fibers, projectional fibers like cortico-spinal tract and optic radiation) at the neonatal period has the most mature fiber organization (low ODI, highest CHARMED-light and NODDI $\nu_{ia/n}$). No significant difference was found in $\nu_{ia/n}$ between the plic and the corpus-callosum, which is unmyelinated at birth (Yakovlev and Lecours, 1967). Only NODDI, based on the orientation dispersion, showed that plic has higher ODI values compared to the cc-sp and cc-ge (Fig. 6).

The higher dispersion in plic leads to its lower FA, despite the presence of myelin. The similar $\nu_{ia/n}$ measured in both cc and plic (Fig. 6) could be attributed to the high packing density of axonal fibers in cc, compensating its lack of myelin (only 3.4% of axons are myelinated in the corpus callosum of primate at the time of birth) (LaMantia and Rakic, 1990), compared to the relatively lower packing density of the already myelinated fibers in the plic. This is consistent with ex-vivo findings that provide evidence for the cc to be the most densely packed and organized tract (exceeding the number of fibers present in the adult at least 3.5 times) (LaMantia and Rakic, 1990) yet still unmyelinated during early postnatal development (Yakovlev and Lecours, 1967).

The number of cc fibers is established by competitive elimination and retraction during the first years after birth (LaMantia and Rakic, 1990). Therefore, its high FA at birth accounts for the high packing density of numerous unmyelinated axonal fibers. Furthermore, at the time of birth genu and splenium of cc contain the highest axonal density (1000 axons/μm^2), which is not the case in the adult brain (LaMantia and Rakic, 1990). Regional comparison of axonal composition of cc in newborns showed that genu and body contain less uniform axons (broader span of diameter) while splenium contains thinner and more uniform axons (LaMantia and Rakic, 1990). Also, the body of corpus callosum in the newborn is the only region of corpus callosum that has small portion of myelinated axonal fibers. Additionally, perinatal reorganization of corpus callosum in primates, spanning from last trimester of pregnancy to first few months postnatally, is accomplished by rapid and substantial retraction of axons in genu and body (LaMantia and Rakic, 1990) and slow rate of axonal loss in splenium. In agreement with previously stated, NODDI and CHARMED-light $\nu_{ia/n}$ revealed higher intra-axonal/neurite volume fraction, axonal density, in the splenium of cc when compared to the genu and body (Fig. 6). The speed of axonal retraction through swelling (LaMantia and Rakic, 1990) and destruction (slower rate in cc-sp and rapid in ge-cc) might leave their geometrical structure intact (compact and dense packing of axonal walls or their remnants) but underlie differences seen in $\nu_{ia/n}$ (increased permeability of axonal skeleton) (Fig. 6). Nevertheless, cc measurements were contaminated by the adjacent presence of ventricles, resulting in a contribution about 20% of the isotropic compartments (Table 1), which may influence our findings, especially the intra-neurite volume fraction of these regions.

Compared to the cc, lower ODI values in the plic followed by lower ODI values in alic reflect the spatio-temporal maturation of the white matter by distinguishing the microstructural components of maturing axonal pathways (over production of numerous non-myelinated fibers in cc, tightly packed myelinated fibers plic and non-myelinated ones in alic) (Fig. 6, NODDI-ODI).

The periventricular crossroads of pathways (green arrows, Figs. 3 & 5) and subplate zone, containing short associational U-fibers (Kostović et al., 2014), are areas abundant in hydrophilic extracellular matrix. Furthermore, periventricular crossroads of pathways contain the complex grid of axonal pathways (Judas et al., 2005). Within six periventricular crossroads of pathways the axons run in radial (thalamocortical), sagittal (associative) and transverse (callosal) directions (Judas et al., 2005; Vasung et al., 2011). In the newborn period within the subplate zone (transient fetal zone below the cerebral cortex serving as 'waiting compartment' for axonal fibers), abundant hydrophilic extracellular matrix provides the medium for ingrowth of short

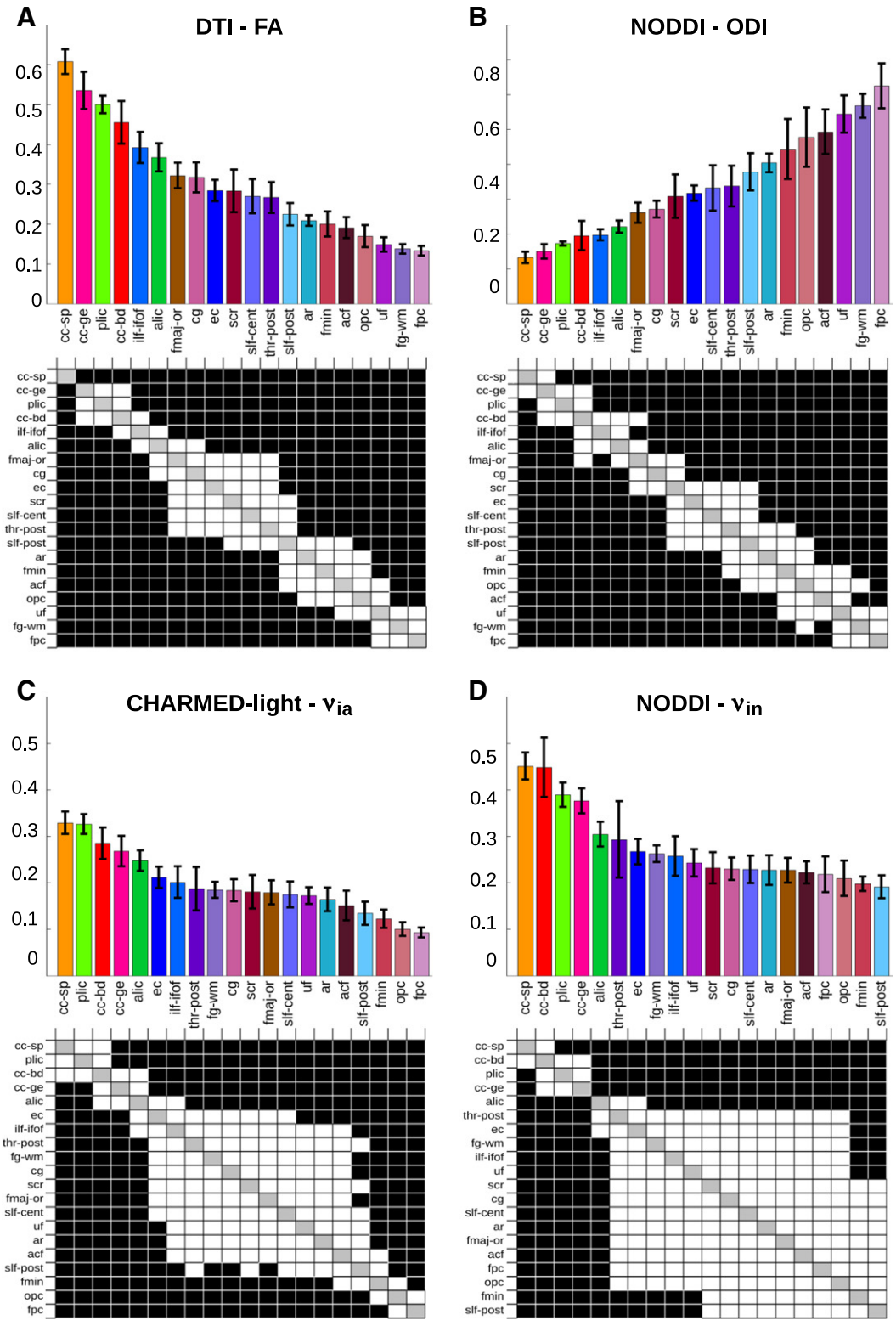

Fig. 6. Bar graphs of model derived parameters averaged over the 13 subjects in the 20 WM ROIs. A. Mean fractional anisotropy (FA) values from DTI model. B. Mean orientation dispersion index (ODI) from the NODDI model. C. Mean intra-axonal volume fraction (ν_{ia}) from the CHARMED-light model. D. Mean intra-neurite volume fraction (ν_{in}) from NODDI. ROIs are rank ordered for each individual metrics (decreasing in A, C and D and increasing in B). Error bars represent the standard deviation over the subjects. Differences between ROIs are shown in binary correlation matrices below the related bar graph. A level of significance was set at $p < 0.05$ with Bonferroni correction for multiple comparison (c.f. the Materials and methods section). Black color: statistically significant; white color: not statistically significant.

associational cortico-cortical fibers (U-fibers), known to mature last (Kostovic and Jovanov-Milosevic, 2006; Kostovic and Rakic, 1990; Kostović et al., 2014; Vasung et al., 2010).

DTI derived parameters provide some evidence of the large extra-neurite space with the smallest FA values and highest diffusivities (Fig. 6 and Table 1) but does not reflect accurately the complex WM

fiber organization of these regions. The compartmented models CHARMED-light and NODDI bring new indices corroborating the cellular architectures known from histology, with the lowest ν_{in}, reflecting the late maturation of these areas with thin non-myelinated fibers, and with highest ODI indicating the presence of fiber crossings and fanning fibers (Fig. 6). Furthermore, CHARMED-light ν_{ia} made a distinction between fpc and opc with the lowest values, as NODDI compensate for the large neurite dispersion in these regions resulting in an intra-neurite volume fraction comparable to most of the other WM regions.

ODI showed statistically significant differences when comparing regions containing short and long associational fibers, with ilf-ifof having the low dispersion index while fg-wm having the highest dispersion index. Furthermore, regions containing not only the long association fibers (ilf-ifof and fmin), but also the external capsule (ec) showed very close $\nu_{ia/n}$ values derived from CHARMED-light and NODDI model. In contrast, regions containing short associational cortico-cortical fibers showed the lowest $\nu_{ia/n}$ values. Therefore large spread in FA values in regions containing late maturing cortico-cortical fibers reflects the microstructure of tightly packed long cortico-cortical pathways (high $\nu_{ia/n}$ values, low dispersion index) and dispersed short cortico-cortical fibers (low $\nu_{ia/n}$ values, high dispersion index, high $\nu_{ea/n}$ values) in the newborn brain.

The multiple cellular sources of the FA values in the developing brain could be identified by CHARMED and NODDI and provide potential microstructural markers of the regional white matter maturation. The periventricular crossroads are the most common sights of injury in premature births (Hüppi, 2004; Perlman, 1998) and are important for the proper axonal guidance and tangential migration of neurons deriving from the ganglionic eminence (Lopez-Bendito et al., 2006; Metin and Godement, 1996). The more precise definition of the cellular changes related to the regional maturation of the connections during the early development is therefore of great value. We suggest that the NODDI model could also assess the protracted intracortical myelination in humans, crucial for development of human specific cognitive abilities (Miller et al., 2012).

Some of the ROIs were contaminated with partial volume with the adjacent ventricles and show significant ν_{iso} values (cc-sp, cc-ge, cc-bd, ilf-ifof). The NODDI reconstruction model in a few other regions also shows that the isotropic compartment contribution may be significant without the presence of CSF or ventricles in the neighborhood (fpc, opc, fmin and the posterior part of the superior longitudinal fasciculus, slf-post).

With the novel CHARMED-light and NODDI parameters we were able to identify microstructural components of (i) early maturing, (ii) partially mature or (iii) immature WM regions of the newborn brain; (i) regions containing tightly packed and myelinated projectional fibers, (ii) regions containing tightly packed unmyelinated fibers such as long associational and callosal cortico-cortical connections and (iii) regions of periventricular crossroads and subcortical white matter containing loosely packed fanning fibers or short cortico-cortical fibers and abundant extracellular space.

Model considerations

The simplifications of the models (Alexander et al., 2010; Panagiotaki et al., 2012; Zhang et al., 2012) and the optimization of the acquisition protocol (Alexander, 2008) to the newborn and clinical environment play an important role in the feasibility of this study. The acquisition time and the maximal b-value were the two main experimental limiting factors. The first one was minimized to avoid motion artifacts and/or an interruption of the acquisition while the newborn wakes up involuntary. Optimization of the b-values utilized in the model was crucial to implement on a clinical scanner, with a theoretical maximum gradient strength of 40 mT/m on our system. The resulted TE of 93 ms was acceptable as newborn brain experiences slower transverse relaxation compared to the adult (Deoni et al., 2012) and thus ensure sufficient SNR for the model fitting. More complex diffusion models, which estimate the axonal diameter (Alexander et al., 2010; Assaf et al., 2008; Barazany et al., 2009; Zhang et al., 2011), would provide very valuable metrics to investigate axonal development, but are too demanding for the current clinical scanners.

The most important simplifications were made with respect to the external compartment in the two models. The constraint of a symmetric diffusion ellipsoid and a tortuosity model for the radial diffusivity, mean the external compartment properties is indirectly estimated from the intra-neurite compartment metrics. These hypotheses may be invalid in the newborn brain, where the extra-neurite space is larger than in the adult due to the lack of myelin, and thus the coupling between the intra- and extra-neurite may be weaker. However, in the very immature regions fpc and opc, NODDI overcame the problem with a significant contribution of the isotropic compartment to account for the large extra-neurite space of these regions (green arrows, Fig. 3). It also demonstrates the large flexibility of this model with only five free parameters to model the underlying architecture.

Another limitation, common to all compartment models, occurs in region with crossing fibers, where a single intra-neurite compartment is not sufficient to capture the true fiber bundles organization. Even though neither CHARMED-light nor NODDI can distinguish multiple distinct fiber bundles inside a single voxel, the ODI of NODDI provides an indication of the presence of multiple fiber bundles with higher estimates (e.g. fpc, opc and uf, Table 1) than regions known to have a single fiber population (e.g. cc, plic and cing). This problem might however be solved by using algorithm to estimate the number of distinct fiber bundles per voxel (e.g. Alexander et al., 2002), to set the number of intra-neurite compartments prior to fitting in combination with extensions to the NODDI and CHARMED-light models to include multiple fiber populations.

Recent development has shown that the acquisition protocol could be simplified and include only two b-value shells and that the maximal b-value could be reduced to 2000 s/mm^2 (Zhang et al., 2012; Winston et al., 2014). The reduction of the number of shells will allow a denser distribution of the diffusion gradient sampling directions in the remaining shells and improve fiber orientation and dispersion estimation. By reducing the maximal b-value, the sequence echo-time could be also shorten and thus result in higher SNR.

Conclusions

In conclusion, we demonstrate the application of multi-compartment models to separate the microstructural factors contributing to the DTI findings in newborns, and the development of connections, which include fiber density, thickness, degree of myelination and fiber geometry like fanning or dispersion.

With the novel CHARMED-light and NODDI parameters we were able to identify microstructural components of early maturing (myelinated and tightly packed plic), partially mature (long associational and callosal cortico-cortical connections having the tightly packed unmyelinated fibers) and immature (short cortico-cortical fibers and periventricular crossroad of pathways having the less tightly packed and incoherently oriented fibers surrounded with abundant extracellular space) white matter regions of the newborn brain.

We also propose a complete processing pipeline using open source software including the generation of study-specific DT template to the reconstruction of advanced diffusion models such as CHARMED-light and NODDI.

The limited spread of age between subjects and the unique time point at term equivalent age assessed in the current study restrained the investigation of developmental changes in specific fiber tracts. Therefore, future work should focus on the acquisition of longitudinal data-sets to follow the development and to provide more precise evolution of the microstructural metrics. In addition, the extension of the NODDI model to the gray matter with its ODI parameter is believed to

bring new insights on the cortical maturation, especially about the dendritic aborization and intracortical myelination.

Acknowledgments

We would like to thank Carole Salomon, Alexandra Darque and Lara Lordier, who took care of the newborn during the acquisition and of the recruitment, making this study feasible.This work is supported by the future and emerging technologies (FET) program of the EU FP7 framework through the CONNECT consortium (www.brain-connect.eu); and the Leenaards and Jeantet Foundations and the Centre d'Imagerie Biomédicale (CIBM) from the UNIL, UNIGE, HUG, CHUV, and EPFL. PSH is additionally funded by the Swiss National Science Foundation 33CM30_140334 (From Cortex to Classroom) and SNF 32473B_135817. DCA is additionally funded by EPSRC under grant EP/E007748.

References

Alexander, D.C., 2008. A general framework for experiment design in diffusion MRI and its application in measuring direct tissue-microstructure features. Magn. Reson. Med. 60, 439–448.

Alexander, D.C., Barker, G.J., Arridge, S.R., 2002. Detection and modeling of non-Gaussian apparent diffusion coefficient profiles in human brain data. Magn. Reson. Med. 48, 331–340.

Alexander, D.C., Hubbard, P.L., Hall, M.G., Moore, E.A., Ptito, M., Parker, G.J.M., Dyrby, T.B., 2010. Orientationally invariant indices of axon diameter and density from diffusion MRI. Neuroimage 52, 1374–1389.

Assaf, Y., Basser, P.J., 2005. Composite hindered and restricted model of diffusion (CHARMED) MR imaging of the human brain. Neuroimage 27, 48–58.

Assaf, Y., Blumenfeld-Katzir, T., Yovel, Y., Basser, P.J., 2008. AxCaliber: a method for measuring axon diameter distribution from diffusion MRI. Magn. Reson. Med. 59, 1347–1354.

Baratti, C., Barnett, A.S., Pierpaoli, C., 1999. Comparative MR imaging study of brain maturation in kittens with T1, T2, and the trace of the diffusion tensor. Radiology 210, 133–142.

Barazany, D., Basser, P.J., Assaf, Y., 2009. In vivo measurement of axon diameter distribution in the corpus callosum of rat brain. Brain 132, 1210–1220.

Bashat, D.B., Kronfeld-Duenias, V., Zachor, D.A., Ekstein, P.M., Hendler, T., Tarrasch, R., Even, A., Levy, Y., Sira, L.B., 2007. Accelerated maturation of white matter in young children with autism: a high b value DWI study. Neuroimage 37, 40–47.

Basser, P.J., Mattiello, J., LeBihan, D., 1994. MR diffusion tensor spectroscopy and imaging. Biophys. J. 66, 259–267.

Beaulieu, C., 2009. Chapter 6 — the biological basis of diffusion anisotropy. In: Heidi, J.-B., Timothy, E.J.B. (Eds.), Diffusion MRI. Academic Press, San Diego, pp. 105–126.

Behrens, T.E.J., Woolrich, M.W., Jenkinson, M., Johansen-Berg, H., Nunes, R.G., Clare, S., Matthews, P.M., Brady, J.M., Smith, S.M., 2003. Characterization and propagation of uncertainty in diffusion-weighted MR imaging. Magn. Reson. Med. 50, 1077–1088.

Brody, B.A., Kinney, H.C., Kloman, A.S., Gilles, F.H., 1987. Sequence of central nervous system myelination in human infancy. I. An autopsy study of myelination. J. Neuropathol. Exp. Neurol. 46, 283–301.

Bullmore, E., Sporns, O., 2009. Complex brain networks: graph theoretical analysis of structural and functional systems. Nat. Rev. Neurosci. 10, 186–198.

Cook, P.A., Bai, Y., Nedjati-Gilani, S., Seunarine, K., Hall, M.G., Park, G.J., Alexander, D.C., 2006. Camino: open-source diffusion-MRI reconstruction and processing. 14th Scientific Meeting of the International Society for Magnetic Resonance in Medicine, Seatle.

Deoni, S.C.L., Dean, D.C., O'Muircheartaigh, J., Dirks, H., Jerskey, B.A., 2012. Investigating white matter development in infancy and early childhood using myelin water faction and relaxation time mapping. Neuroimage 63, 1038–1053.

Dubois, J., Hertz-Pannier, L., Dehaene-Lambertz, G., Cointepas, Y., Bihan, D.L., 2006. Assessment of the early organization and maturation of infants' cerebral white matter fiber bundles: a feasibility study using quantitative diffusion tensor imaging and tractography. Neuroimage 30, 1121–1132.

Dyrby, T.B., Søgaard, L.V., Hall, M.G., Ptito, M., Alexander, D.C., 2013. Contrast and stability of the axon diameter index from microstructure imaging with diffusion MRI. Magn. Reson. Med. 70, 711–721.

Flechsig Of Leipsic, P., 1901. Developmental (myelogenetic) localisation of the cerebral cortex in the human subject. Lancet 158, 1027–1030.

Forbes, K.P.N., Pipe, J.G., Bird, C.R., 2002. Changes in brain water diffusion during the 1st year of life. Radiology 222, 405–409.

Gilmore, J.H., Lin, W., Corouge, I., Vetsa, Y.S.K., Smith, J.K., Kang, C., Gu, H., Hamer, R.M., Lieberman, J.A., Gerig, G., 2007. Early postnatal development of corpus callosum and corticospinal white matter assessed with quantitative tractography. AJNR Am. J. Neuroradiol. 28, 1789–1795.

Huang, H., Jeon, T., Sedmak, G., Pletikos, M., Vasung, L., Xu, X., Yarowsky, P., Richards, L.J., Kostovic, I., Sestan, N., Mori, S., 2013. Coupling diffusion imaging with histological and gene expression analysis to examine the dynamics of cortical areas across the fetal period of human brain development. Cereb. Cortex 23, 2620–2631.

Hüppi, P.S., 2004. Immature white matter lesions in the premature infant. J. Pediatr. 145, 575–578.

Hüppi, P.S., Dubois, J., 2006. Diffusion tensor imaging of brain development. Semin. Fetal Neonatal Med. 11, 489–497.

Hüppi, P.S., Maier, S.E., Peled, S., Zientara, G.P., Barnes, P.D., Jolesz, F.A., Volpe, J.J., 1998. Microstructural development of human newborn cerebral white matter assessed in vivo by diffusion tensor magnetic resonance imaging. Pediatr. Res. 44, 584–590.

Hüppi, P.S., Murphy, B., Maier, S.E., Zientara, G.P., Inder, T.E., Barnes, P.D., Kikinis, R., Jolesz, F.A., Volpe, J.J., 2001. Microstructural brain development after perinatal cerebral white matter injury assessed by diffusion tensor magnetic resonance imaging. Pediatrics 107, 455–460.

Inder, T., Huppi, P.S., Zientara, G.P., Maier, S.E., Jolesz, F.A., di Salvo, D., Robertson, R., Barnes, P.D., Volpe, J.J., 1999. Early detection of periventricular leukomalacia by diffusion-weighted magnetic resonance imaging techniques. J. Pediatr. 134, 631–634.

Jespersen, S.N., Leigland, L.A., Cornea, A., Kroenke, C.D., 2012. Determination of axonal and dendritic orientation distributions within the developing cerebral cortex by diffusion tensor imaging. IEEE Trans. Med. Imaging 31, 16–32.

Judaš, M., 2011. Prenatal development of the human fetal telencephalon. In: Prayer, D. (Ed.), Fetal MRI. Springer, Berlin Heidelberg, pp. 81–146.

Judas, M., Rados, M., Jovanov-Milosevic, N., Hrabac, P., Stern-Padovan, R., Kostovic, I., 2005. Structural, immunocytochemical, and MR imaging properties of periventricular crossroads of growing cortical pathways in preterm infants. AJNR Am. J. Neuroradiol. 26, 2671–2684.

Judaš, M., Šimić, G., Petanjek, Z., Jovanov-Milošević, N., Pletikos, M., Vasung, L., Vukšić, M., Kostović, I., 2011. The Zagreb Collection of human brains: a unique, versatile, but underexploited resource for the neuroscience community. Ann. N. Y. Acad. Sci. 1225 (Suppl. 1), E105–E130.

Kang, H.J., Kawasawa, Y.I., Cheng, F., Zhu, Y., Xu, X., Li, M., Sousa, A.M., Pletikos, M., Meyer, K.A., Sedmak, G., Guennel, T., Shin, Y., Johnson, M.B., Krsnik, Z., Mayer, S., Fertuzinhos, S., Umlauf, S., Lisgo, S.N., Vortmeyer, A., Weinberger, D.R., Mane, S., Hyde, T.M., Huttner, A., Reimers, M., Kleinman, J.E., Sestan, N., 2011. Spatio-temporal transcriptome of the human brain. Nature 478, 483–489.

Kostovic, I., Jovanov-Milosevic, N., 2006. The development of cerebral connections during the first 20–45 weeks' gestation. Semin. Fetal Neonatal Med. 11, 415–422.

Kostovic, I., Rakic, P., 1990. Developmental history of the transient subplate zone in the visual and somatosensory cortex of the macaque monkey and human brain. J. Comp. Neurol. 297, 441–470.

Kostović, I., Jovanov-Milošević, N., Radoš, M., Sedmak, G., Benjak, V., Kostović-Srzentić, M., Vasung, L., Culjat, M., Radoš, M., Hüppi, P., Judaš, M., 2014. Perinatal and early postnatal reorganization of the subplate and related cellular compartments in the human cerebral wall as revealed by histological and MRI approaches. Brain Struct. Funct. 219, 231–253.

Kunz, N., Zhang, H., Assaf, Y., Lazeyras, F., Alexander, D., Huppi, P.S., 2013. Brain Microstructure Assessed by CHARMED and NODDI in the Newborn. In: Proceedings of the 21st International Society for Magnetic Resonance in Medicine, Utah, p. 0796.

LaMantia, A.S., Rakic, P., 1990. Axon overproduction and elimination in the corpus callosum of the developing rhesus monkey. J. Neurosci. 10, 2156–2175.

Lopez-Bendito, G., Cautinat, A., Sanchez, J.A., Bielle, F., Flames, N., Garratt, A.N., Talmage, D. A., Role, L.W., Charnay, P., Marin, O., Garel, S., 2006. Tangential neuronal migration controls axon guidance: a role for neuregulin-1 in thalamocortical axon navigation. Cell 125, 127–142.

Metin, C., Godement, P., 1996. The ganglionic eminence may be an intermediate target for corticofugal and thalamocortical axons. J. Neurosci. 16, 3219–3235.

Miller, D.J., Duka, T., Stimpson, C.D., Schapiro, S.J., Baze, W.B., McArthur, M.J., Fobbs, A.J., Sousa, A.M., Sestan, N., Wildman, D.E., Lipovich, L., Kuzawa, C.W., Hof, P.R., Sherwood, C.C., 2012. Prolonged myelination in human neocortical evolution. Proc. Natl. Acad. Sci. U. S. A. 109, 16480–16485.

Neil, J.J., Shiran, S.I., McKinstry, R.C., Schefft, G.L., Snyder, A.Z., Almli, C.R., Akbudak, E., Aronovitz, J.A., Miller, J.P., Lee, B.C.P., Conturo, T.E., 1998. Normal brain in human newborns: apparent diffusion coefficient and diffusion anisotropy measured by using diffusion tensor MR imaging. Radiology 209, 57–66.

Panagiotaki, E., Schneider, T., Siow, B., Hall, M.G., Lythgoe, M.F., Alexander, D.C., 2012. Compartment models of the diffusion MR signal in brain white matter: a taxonomy and comparison. Neuroimage 59, 2241–2254.

Partridge, S.C., Mukherjee, P., Henry, R.G., Miller, S.P., Berman, J.I., Jin, H., Lu, Y., Glenn, O.A., Ferriero, D.M., Barkovich, A.J., Vigneron, D.B., 2004. Diffusion tensor imaging: serial quantitation of white matter tract maturity in premature newborns. Neuroimage 22, 1302–1314.

Paus, T., Collins, D.L., Evans, A.C., Leonard, G., Pike, B., Zijdenbos, A., 2001. Maturation of white matter in the human brain: a review of magnetic resonance studies. Brain Res. Bull. 54, 255–266.

Penny, W.D., 2012. Comparing dynamic causal models using AIC, BIC and free energy. Neuroimage 59, 319–330.

Perlman, J.M., 1998. White matter injury in the preterm infant: an important determination of abnormal neurodevelopment outcome. Early Hum. Dev. 53, 99–120.

Pierpaoli, C., Jezzard, P., Basser, P.J., Barnett, A., Di Chiro, G., 1996. Diffusion tensor MR imaging of the human brain. Radiology 201, 637–648.

Provenzale, J.M., Isaacson, J., Chen, S., Stinnett, S., Liu, C., 2010. Correlation of apparent diffusion coefficient and fractional anisotropy values in the developing infant brain. AJ. Am. J. Roentgenol. 195, W456–W462.

Reese, T.G., Heid, O., Weisskoff, R.M., Wedeen, V.J., 2003. Reduction of eddy-current-induced distortion in diffusion MRI using a twice-refocused spin echo. Magn. Reson. Med. 49, 177–182.

Stanisz, G.J., Szafer, A., Wright, G.A., Henkelman, R.M., 1997. An analytical model of restricted diffusion in bovine optic nerve. Magn. Reson. Med. 37, 103–111.

Szafer, A., Zhong, J., Gore, J.C., 1995. Theoretical model for water diffusion in tissues. Magn. Reson. Med. 33, 697–712.

Vasung, L., Huang, H., Jovanov-Milošević, N., Pletikos, M., Mori, S., Kostović, I., 2010. Development of axonal pathways in the human fetal fronto-limbic brain: histochemical characterization and diffusion tensor imaging. J. Anat. 217, 400–417.

Vasung, L., Jovanov-Milošević, N., Pletikos, M., Mori, S., Judaš, M., Kostović, I., 2011. Prominent periventricular fiber system related to ganglionic eminence and striatum in the human fetal cerebrum. Brain Struct. Funct. 215, 237–253.
Vasung, L., Fischi-Gomez, E., Hüppi, P.S., 2013. Multimodality evaluation of the pediatric brain: DTI and its competitors. Pediatr. Radiol. 43, 60–68.
Wang, Y., Gupta, A., Liu, Z., Zhang, H., Escolar, M.L., Gilmore, J.H., Gouttard, S., Fillard, P., Maltbie, E., Gerig, G., Styner, M., 2011. DTI registration in atlas based fiber analysis of infantile Krabbe disease. Neuroimage 55, 1577–1586.
Winston, G.P., Micallef, C., Symms, M.R., Alexander, D.C., Duncan, J.S., Zhang, H., 2014. Advanced diffusion imaging sequences could aid assessing patients with focal cortical dysplasia and epilepsy. Epilepsy Research 108, 336–339.
Yakovlev, P.A., Lecours, I.R., 1967. The myelogenetic cycles of regional maturation of the brain. In: Minkowski, A. (Ed.), Regional Development of the Brain in Early Life. Blackwell, Oxford.
Zhang, H., Yushkevich, P.A., Alexander, D.C., Gee, J.C., 2006. Deformable registration of diffusion tensor MR images with explicit orientation optimization. Med. Image Anal. 10, 764–785.
Zhang, H., Hubbard, P.L., Parker, G.J.M., Alexander, D.C., 2011. Axon diameter mapping in the presence of orientation dispersion with diffusion MRI. Neuroimage 56, 1301–1315.
Zhang, H., Schneider, T., Wheeler-Kingshott, C.A., Alexander, D.C., 2012. NODDI: practical in vivo neurite orientation dispersion and density imaging of the human brain. Neuroimage 61, 1000–1016.